Smart load management of water injection systems in offshore oil and gas platforms integrating wind power

Santiago Sanchez[1,*], Elisabetta Tedeschi[2], Jesus Silva[3], M. Jafar[4], A. Marichalar[5]

[1]Norwegian University of Science and Technology
[2]Norwegian University of Science and Technology
[3]Norwegian University of Science and Technology
[4]DNV GL
[5]DNV GL
[*]santiago.sanchez@ntnu.no

Abstract: The high pollution coming from the use of gas turbines in oil and gas (O&G) platforms is calling for more sustainable solutions. One of those is to use wind turbines (WT) to supply power to the water injection systems (WIS) of offshore O&G installations and explore the potential of smart energy management in providing more efficient and green solutions to the O&G sector. The effect of WT integration into the local power system and the coordination with the local gas turbines, need to be carefully analysed since the natural intermittency of the wind resource can jeopardize the stability and efficiency of the offshore grid. In general, the existence of flexible loads interfaced by variable speed drives (VSD), such as water injection systems, can help overcome some of the challenges related to wind intermittency and local rotor angle stability: suitable control of such non-essential loads and load segregation can be implemented to reduce the effect of wind power fluctuations, balance power generation and consumption and contribute to maintaining the optimal efficiency of the gas turbine adjusting its loading conditions. The basic assumption is that the WIS can follow the generation available from the wind turbines. The assumption is reasonable since WISs do not require a fixed injection rate. This work will investigate the system dynamics in the event of short-term wind-induced power fluctuations, analysing the evolution of electrical variables, such as active power and generator rotor speed/frequency, under different operating conditions, to specifically evaluate the possible arise of low-frequency oscillations. The impact of an adequate WIS load control to counteract wind variations and increase the system damping is also further explored. Moreover, in order to prevent the event of critical rotor oscillations in the gas turbine and other directly-connected rotating machines due to the WT dynamics, an algorithm for system damping estimation is proposed and its performance studied in the selected test cases.

1. Introduction

The need of sustainability at global level encourages the implementation of greener solutions, especially in the most polluting industrial sectors. The will of reducing CO_2/NO_x emissions from oil and gas installations, along with the difficulty of deploying new gas turbines to supply increasing loads due to space and structural constraints on the platforms, makes the idea of integrating wind turbines to O&G attractive. This paper, in particular, investigates the possibility of using wind power to supply the platform water-injection systems, similarly to the concept proposed by DNV

GL in the WinWin project [1]. The objective of the water injection system is to inject raw seawater or processed water in order to pressurize the well and consequently increase the oil recovery rate (ORR) using the energy generated locally by the wind turbines. The DNV GL technical assessment considered a stand-alone WIS, not connected to the platform, where the main subsystem were the wind turbine and the mechanical set-up composed of a VSD and an induction motor. Here, the solution proposed is a hybrid configuration, where a floating wind turbine is integrated into the existing power system based on gas turbines, allowing retrofitting of existing installations. The wind turbine works in parallel with the gas turbines and it supplies a flexible load that represents a water injection pump. However, as indicated in [2], there are several challenges associated with wind power integration that might affect the secure and stable operation of the O&G platform power system. Those of main interest in this work are the system dynamics due to the wind variability and power fluctuations affecting the frequency and voltage of the O&G platform.

2. State of the art

The integration of wind power into O&G platforms was investigated only relatively recently, and still a limited number of contributions is available on the topic. Some of the previous studies [3–5] targeted electrified O&G installations, in particular those being interconnected to the main power system through an HVDC link, and excluding the presence of a gas turbines on the platform itself. Dynamics and stability issues of such hybrid AC/DC systems, as well as their most relevant operational scenarios, are inherently different from those of an isolated system, such as the one analyzed in this paper. Among the studies focusing on an isolated system, [6] performs voltage and frequency stability analysis checking grid code compliance under two critical scenarios, such as loss of load and load start-up. Ref. [7] performs similar analyses considering the integration of a wind farm of up to 100 MW into an O&G cluster: the paper considers additional operational scenarios, such as loss of generation (by disconnection of the wind farm or of the gas turbine) and includes loss analyses. Ref. [8] also includes voltage and frequency stability analyses with similar focus, but extends the range of considered scenarios to load start-up, loss of wind generation and of interconnection, and includes the quantification of CO2 and NOx emission reduction due to the wind integration. Unlike the present paper, however, all the above mentioned contributions do not take into account the effects of the short-term wind power variability. Effect of wind intermittency and realistic wind power profiles, have only been considered in [9, 10]. While [9] is a pure energy analysis, with no transient stability considerations, ref. [10] is the only contribution targeting voltage and frequency stability analysis under rapidly varying generation condition. As for [8], such analysis is, however, only aimed at ensuring grid code compliance of the voltage and frequency profiles, according to the IEC-61892 standard for electrical installations in mobile and fixed offshore units. To the knowledge of the authors, none of the previous contributions has focused on another aspect that can be fundamental to ensure the proper operation of wind-powered O&G installations, i.e. the possible arise of electro-mechanical, low-frequency, oscillations, which can jeopardize, not only the efficiency, but also the overall stability of the considered system.

The paper is organized as follows: section 3 frames the problem and highlights its relevance. Section 4 presents the O&G platform power system and its components. Section 5 describes the scenarios used to test the system, section 6 presents the damping coefficient theory and tests on the main test cases. Finally, section 7 presents the conclusions of the paper and the appendices present the parameters of the components used in the O&G power system.

3. Relevance of the investigated problem and contributions of the paper

The problem of electro-mechanical oscillations has been widely investigated in traditional large-scale power systems. Such low frequency oscillations, in a range between 0.1 and 2 Hz, are caused by instantaneous unbalances between generated and consumed power, and they result in rotor angle oscillations of the electrical generators connected to the grid [11]. In particular, oscillations in the range 0.1 to 0.7 Hz are considered the most critical ones, and several cases in which they have led to protection and generation tripping, and eventually to major blackouts, have been reported [11].
In addition to these system-level consequences of low frequency oscillations, they can provoke "*fatigue of machine shafts, cause excessive wear of mechanical actuators of machine controllers*" [12] and decrease the efficiency of system operation, by affecting most of the interconnected components.
In particular, electro-mechanical oscillations can lead to abnormal stresses in, and damage to, the generator-turbine shaft [13], and, in the considered O&G installation, this could impact the main gas turbine group.

This phenomenon, however, would not affect only the generators, since it has been shown that energy oscillations can occur between generators and induction motors [14], and they can be amplified under certain conditions, depending on the respective phase of the potential and kinetic energy of the rotating masses. This can affect all the ac induction motors directly connected to the O&G distribution system, whose share can vary depending on the specific platform [3].
In [15] it was specifically shown that low-frequency (sub-harmonic) oscillations have an adverse effect on induction motor performances even if present with very small amplitudes. They potentially lead to reduced speed stability, and eventually result in saturation of the magnetic circuit with subsequent overcurrents that can damage the machine.
In addition, significant share of the O&G platform power demand is composed of boilers and heaters [3], which, as thermostatically controlled loads, are considered potential contributors to low-frequency instability problems [11].
For all the above reasons, and due to the criticality and high reliability of operation required in O&G platforms, it is considered especially important to assess the possible arise and amplification of such electro-mechanical oscillations, when intermittent wind power is integrated. The risk of grid instabilities due of such phenomenon is inherently depended on the frequency of the induced oscillations, also when their amplitude (and consequently that of related frequency fluctuations) is very limited [16].
Moreover, while squirrel cage wind generators have a damping effect on the interconnected power system, this is not true for WT interfaced with a back-to-back converter, as the one considered in this paper [17]. For wind turbines using full-rated power electronics the effect of wind power on low frequency oscillations becomes more ambiguous [17] and requires careful evaluation also in the case of grid interconnected systems.

The scope of the paper is, firstly, to evaluate the impact of the intermittent wind power injection on the local O&G distribution systems, in terms of induced low-frequency [0.1 -2 Hz] oscillations, and stress the importance of their early detection. For this purpose, the criticalities of the considered electric system are first analysed in detail. As mentioned before, main O&G platforms present standard operation based on synchronous generator (SG) and gas turbine dynamics, as well as different types of loads, and WT integration can increase the oscillations in the rotor of

the synchronous generator and of other directly connected ac motors. The rotor transients with under-damped oscillations cause the risk that an unstable oscillation appears producing a system collapse. For this purpose, the damping level of the system is analised both without and with wind power integration.

Moreover, the possibility of using a smart load management by flexibly controlling the WIS load to follow the generation is explored as a way to reduce such electro-mechanical oscillations and evaluate the system damping. WIS motors, if controlled adequately, can play an active role in counteracting the wind variability and help maintaining the system power balance. As explained in [18], this type of motors are equipped with variable speed drives, which are flexible units adjustable to different operating points or injection rates, and consequently adaptable to multiple demand levels. The idea proposed here exploits the load flexibility of the WIS to keep a stable and efficient system operation, ensuring the minimum possible impact to the existing grid, by acting mainly on controllable and non-critical loads. This concept has been previously explored in [19] with a focus on voltage and frequency stability, but it is investigated for its possible contribution to rotor angle stability in the present article.

Once proved the criticality of electro-mechanical oscillations and suggested smart load management as mitigation action, this paper proposes, as third contribution, a simplified semi-recursive algorithm to estimate the damping coefficient of the low-frequency oscillations, which can be used to set a warning alarm to protect sensitive components in the O&G platform. A discussion on the challenges of its implementation is also included.

4. Power system for O&G platforms with WIS

The electrical power system of an O&G platform with an integrated wind power generator is schematically shown in Fig. 1. The system consists of a floating wind turbine, the cable, two transformers T_1 and T_2, a gas turbine (GT) with a synchronous generator (SG) at the O&G platform, and subsea WIS based on VSD motor which, in the following analysis, is represented in a simplified way as a flexible load. A fixed load takes into account the base load consumption of the platform. The main system components are presented in the following subsections. Additionally, the proposed strategy is to follow with the flexible load the wind turbine power injection profile; this can be done by the use of a communications link based on industrial protocols (e.g. the link is the line between the AC/AC converters and flexible load in Fig. 1).

4.1. Gas turbine (GT)

Gas turbines represent the conventional power supply for O&G platforms, closely integrated with the electric generator. Their thermal efficiency is low, around 30%. In some cases, they are equipped with secondary recovery system to extract residual energy normally in the form of heat. If the wasted heat is recovered, the efficiency can go up to 60% by a steam engine. However, this is not the common solution found in O&G. In Norway, the greenhouse gas emissions from oil and gas installations was 15 million tonnes of CO2 equivalent in 2015, corresponding to 28% of the total domestic emissions [20]. This is driving increasing efforts for their reduction.
The gas turbine and the connected synchronous generator present the configuration shown in Fig. 2. The active power injected into the grid is P_{egt}, the reactive power is Q_{egt}, the mechanical power from the GT is P_{mgt}, the corresponding power reference input of the GT is P_{mref}, the rotor angular

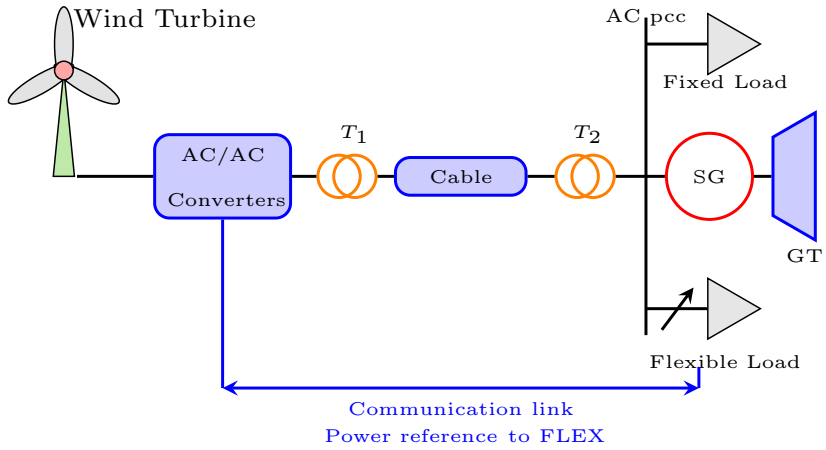

Fig. 1. *O&G platform with wind turbine and WIS.*

speed of the generator is ω_r, the field voltage is E_{field}, the grid voltage at the terminals is V_{ggt}. The model of the gas turbine is based on the combustion turbine described in [21]: it is a dynamic model of first order with time constant T_{gt} (Fig. 3), so the transfer function of the GT is $G_{gt} = 1/(T_{gt}s + 1)$. The SG used in this paper is the well known simplified synchronous machine third order model [21–24]. The excitation system is an IEEE type 1 and the model is implemented according to the recommendations in [23]. The synchronous generator (SG) has transfer function $1/(2Hs + k_{damp})$, H is the inertia constant in seconds and k_{damp} is the damping coefficient of the generator axis [25]. A pure proportional controller ($H_{c\omega} = \frac{H}{T_{gt}}$) is sufficient and it is developed based on the modulus optimum strategy [26] applied to the open loop transfer function $G_{gtOL} = (1/(T_{gt}s + 1))(1/(2Hs + k_{damp}))$.

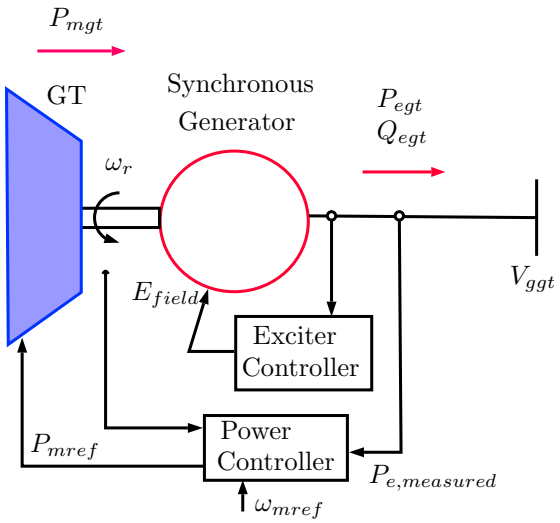

Fig. 2. *Gas turbine and synchronous generator configuration.*

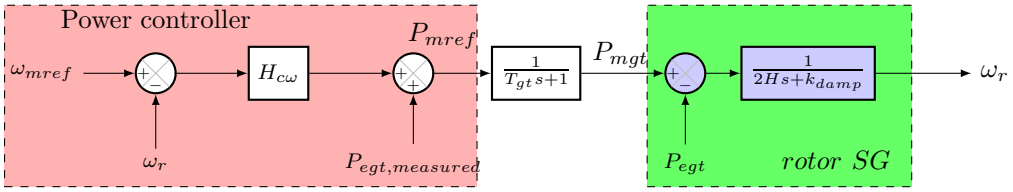

Fig. 3. *Gas turbine and synchronous generator mechanical model and control strategy.*

4.2. Water injection system

When an oil well is discovered oil flows naturally out of the reservoir during the first exploitation phase. Primary production usually recovers only 30 to 35 % of the oil in place. As time passes the pressure starts to decline and the production decreases. The well must then be intervened for pressure support. This is called secondary recovery or enhanced oil recovery (EOR), and the objective is to provide energy artificially to boost a declining production in a mature field. There are two techniques for secondary EOR process: water injection or gas lift. The latter consists of injecting gas instead of water and it depends on the physical characteristics of the formation. It is attractive when high pressure gas is available without compression or when gas cost is low. Compressors are sensitive to downtime and are not suitable for a fluctuating power source [27]. In other cases water injection is preferable. Water injection effectiveness varies according to the formation characteristics, it can recover anywhere from 5% to 50% of the remaining oil, enhancing the well economics. When the water content in relation to oil reaches 90 to 99%, the process becomes uneconomical [27]. Another form of water injection consists of introducing heated water. This is attractive for reservoirs with heavy oil content, since heat helps decreasing oil viscosity and making it more fluid [28].

4.2.1. Flexible load (FLEX): In this paper the WIS is represented as a flexible load. A flexible load is a load whose active and reactive power can change over time according to a predefined profile. This is modelled by a device that allows independent control of active (P_{FLEX}) and reactive (Q_{FLEX}) power. The corresponding apparent power is S_{FLEX}. In the simulation in this paper the load is assumed purely active, hence Q_{FLEX} is set to zero.

4.3. Fixed load (FL)

The fixed load represents lighting, heating and comfort loads on the platform. It also includes systems losses and other passive elements. The model representation of a fixed load uses parallel combination of different RLC elements. The resulting impedance is modelled as a constant impedance load at a given nominal frequency f_e. A three-phase balanced load with no capacitive elements is selected for the considered application [29]. It can be represented as Z_{load} equal to a resistive load R_{load} in parallel with an inductive load ($j\omega_e L_{load}$); where ω_e is the electrical speed. The load consumes active and reactive power; according to the following relationships:

$$\begin{aligned} P_{FL} &= \frac{V^2}{R_{load}}, \\ Q_{FL} &= \frac{V^2}{\omega_e L_{load}}, \end{aligned} \tag{1}$$

where V is the nominal voltage at the load terminals, P_{FL} and Q_{FL} are the active and reactive power of the fixed passive load, respectively with apparent power S_{FL}.

4.4. Wind power system

The wind turbine considered in this study is a 6 MW wind turbine interfaced to the grid by a back-to-back power converter, and it resembles the operation of the HyWind floating turbine [30]. The configuration of the system is shown in Fig. 4, and it is connected to the transformer T_1. The wind speed is represented by v_{wind}, the generator axis rotor speed is ω, the grid converter controller uses the grid voltage v_g, the AC current i and the voltage references e, for power conditioning on the grid side. The power P_{wt} is the electric power that the WT injected into the grid. Furthermore, when the smart load management is applied the $P_{reference}$ is the power reference in pu sent to the flexible load by a communication link. The corresponding simulation model on the WT side consists of a current source (representing the wind turbine, the generator, the MPPT and converter controller). A grid side converter is connected to this system and is used to control the voltage link DC. The power characteristic of the turbine is based on a cut-in speed of 4 m/s (0.16 pu), nominal speed of 12 m/s (0.48 pu) and cut-out speed of 25 m/s (1 pu).

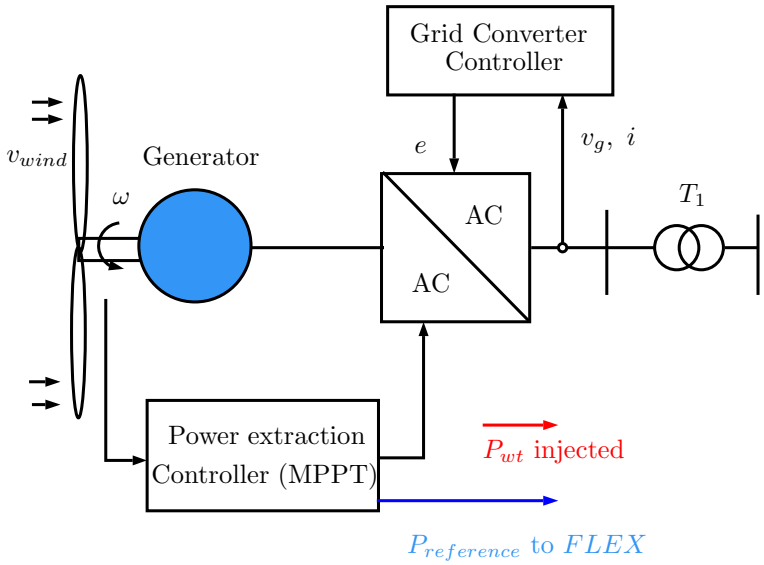

Fig. 4. *Wind turbine configuration and control.*

4.4.1. Rotor side converter control: The main function of the controlled rectifier on the WT rotor side is to control the rotor speed of the generator for maximum power extraction [31, 32].

For modelling purposes, the WT structure is simplified to a current source supplying a PMSG, controlled with an MPPT by the converter controller.

In particular, the MPPT is applied for wind speeds between 4 and 12 m/s, while above the nominal speed the pitch control ensures that the output power is kept constant to the nominal value up to a wind speed of 25 m/s. Above the cut-out speed the WT is shut down for safety reasons.

As a first step the impact of a variable wind speed profile (v_{wind} in Fig. 5) on the power extraction (P_{wt} in Fig. 6) is studied.

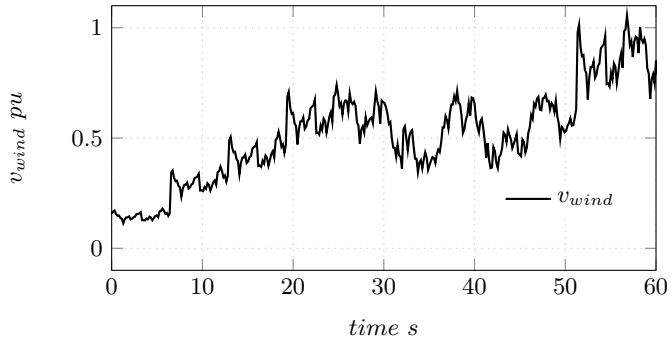

Fig. 5. *Wind speed profile in pu, base wind speed = 25 m/s.*

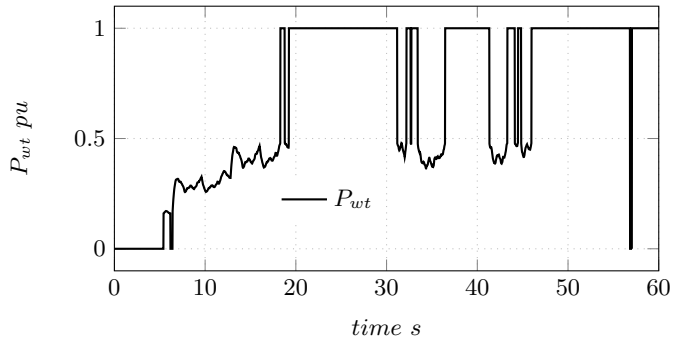

Fig. 6. *Power extracted from the WT in pu, based on the WT rated power ($P_{base} = 6$ MW).*

4.4.2. Grid side converter control: The main objective of the grid side inverter is to transfer maximum power to the local grid by stabilizing the DC link voltage and ensure compliance with the grid requirements. The grid side converter control diagram is depicted in Fig. 7. The control system is developed in the dq synchonous reference frame and is standard for this application and explained in [33]. The voltage in the DC link V_{dc} is measured, squared and compared with the corresponding squared reference V_{dcref}, a PI voltage controller generates a reference current I_{dref} to be compared with the actual current in the d-axis i_d as in (2). A similar controller acting on the q axis current i_q is set such that I_{qref}=0, then only active power is injected and Q_{ref} is set to zero. The corresponding equations are:

$$\begin{aligned} e_d &= H_{ci}(i_{dref} - i_d) - \omega_e L i_q + v_{gd}, \\ e_q &= H_{ci}(i_{qref} - i_q) + \omega_e L i_d + v_{gq}, \\ i_{dref} &= H_{cv}(V_{dcref}^2 - V_{dc}^2) + P_{out} \end{aligned} \tag{2}$$

Both d and q current references enter a current controller with decoupling terms, in order to determine the voltage references $e_{d,q}$, H_{ci} represents the current controller, H_{cv} is the voltage controller system and P_{out} is the output power of the DC link. The dq signals are sent to an inverse Park transformation block to generate the abc frame voltages. The reference angle is extracted from the grid voltage v_g using a PLL block.

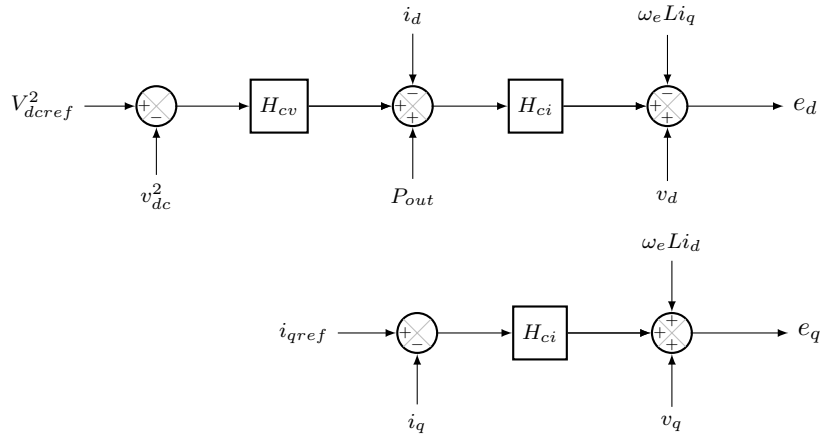

Fig. 7. *Grid side converter control strategy.*

5. Test cases

After considering a base case in which no wind turbine is integrated, the system will be tested under multiple cases (see Table 1) changing the proportion between fixed and flexible load as shown in Fig. 8 in order to analyse the impact of the wind power penetration. The base case (Case I) presents a change in the load ratio S_{FLEX}/S_{FL} in which S_{FLEX} is set to operate at 100% of its nominal power (3 MW -no flexibility used) and S_{FL} is varied in three steps (η_1 in Fig. 8) from 0.3, 0.7 to 0.88 pu (1 pu equal to 25 MVA) and varies from 0 to 22 MVA (Case I). Moreover, the FL is consuming each of the powers indicated above for the time period τ_k with $k \in \{1, 2, 3\}$. This represents a case in which the WIS is running continuously, independently of the local generation and other (fixed) loads on the platform undergo normal operation variations. Case II describes the operation as case I but the WT is included. When a smart load management (SLM) is implemented the WIS is only activated when the WT is producing power i.e. the S_{FLEX} is following the WT profile (Case III), the loads ratio behaves as $\eta_{no-delay}$ in Fig. 8. A final case (Case IV) is analysed in which the flexible operation of the WIS based on the wind power production is affected by a delay (1 s) $\eta_{1s-delay}$ due to the sum of communication and actuators delays.

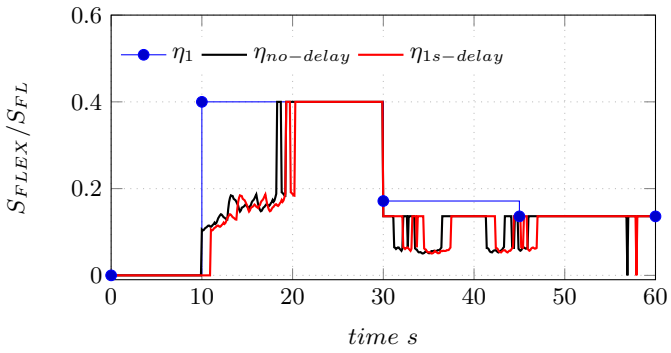

Fig. 8. *Loads ratio (S_{FLEX}/S_{FL}) for the test cases.*

Oscillations of the generator rotor angular speed in the system are studied to obtain an indicator of the possible destabilizing effects and abnormal stresses due to the WT penetration and FLEX load dynamics in the grid [34]. The oscillations may pose a serious threat to system security if they

Table 1 Cases under test for the O&G platform electrical system.

Case	WT	GT	FL for the time ranges ($\tau_1/\tau_2/\tau_3$)	SLM active $\tau_1/\tau_2/\tau_3$	FLEX
I (base case)	NC	25 MW installed, Balancing load	7.5/17.5/22 MVA (0.3/0.7/0.88) pu	no/no/no	3 MW Constant
II	C [0-6] MW	25 MW installed, Balancing load	7.5/17.5/22 MVA (0.3/0.7/0.88) pu	no/no/no	3 MW Constant
III	C [0-6] MW	25 MW installed, Balancing load	7.5/17.5/22 MVA (0.3/0.7/0.88) pu	yes/yes/yes	[0-3] MW follows wind
IV	C [0-6] MW	25 MW installed, Balancing load	7.5/17.5/22 MVA (0.3/0.7/0.88) pu	yes/yes/yes	[0-3] MW follows wind with 1 s delay

Note: τ_1 is from 10-30 s, τ_2 is from 30-45 s and τ_3 is from 45-60 s.
NC:Not connected, C:connected

are not controlled properly [35]. As in other works involving multiple generators the oscillations observed in the system are in a range of [0.1-2] Hz. The frequency spectrum of the oscillations is presented in the following subsections for each test with the Fourier transform of the rotor angular speed at the GT-SG, with the goal of highlight the critical low-frequency contributions.

5.1. Case I: constant FLEX (no WT)

The first test is performed on the O&G power system without the integration of the WT. In this test the voltage in the AC system, the power quantities for GT (i.e. the electrical active P_{egt}, reactive Q_{egt} and mechanical power P_{mgt} of the GT, respectively) are controlled by the GT (Fig. 9). The power consumption of the WIS is kept constant at its nominal power (3 MW) after being activated at 10 s. It represents 12% of the nominal GT power. The passive load is switched in three steps (i.e. three time ranges τ_1, τ_2 and τ_3). In the first part the power consumed by the load is 7.5 MVA (0.3 pu) with PF=0.9848 ($S_{FL,1}$). The active power change at the instant S_{FLEX} is activated is shown in Fig. 9(a), it is important to note that there is no reactive power change and therefore, the grid voltage has a low disturbance (in Fig. 9(b) at 10 s). A 0.4 pu load with PF=0.8660 is added at 30 s ($S_{FL,2}$). The final load added represents 0.18 pu power of the GT with PF=0.9848 and is activated at 45 s ($S_{FL,3}$). The main objective is to analyse the behaviour of the system supplied by the gas turbine only, which is the less environmentally friendly operation, as a base case. The initial operation point is the system feeding the passive load $S_{FL,1}$. The activation of the passive loads causes step changes in the field voltage E_{field} producing the regulation of the grid voltage

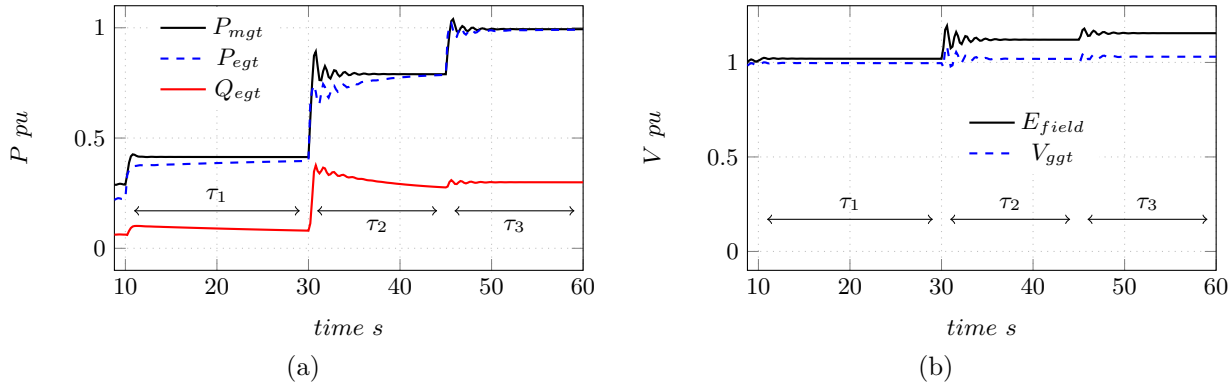

Fig. 9. *System behaviour in the base case (no WT integrated).*
a Mechanical power, active and reactive power of the GT.
b Field voltage and grid voltage of the GT.

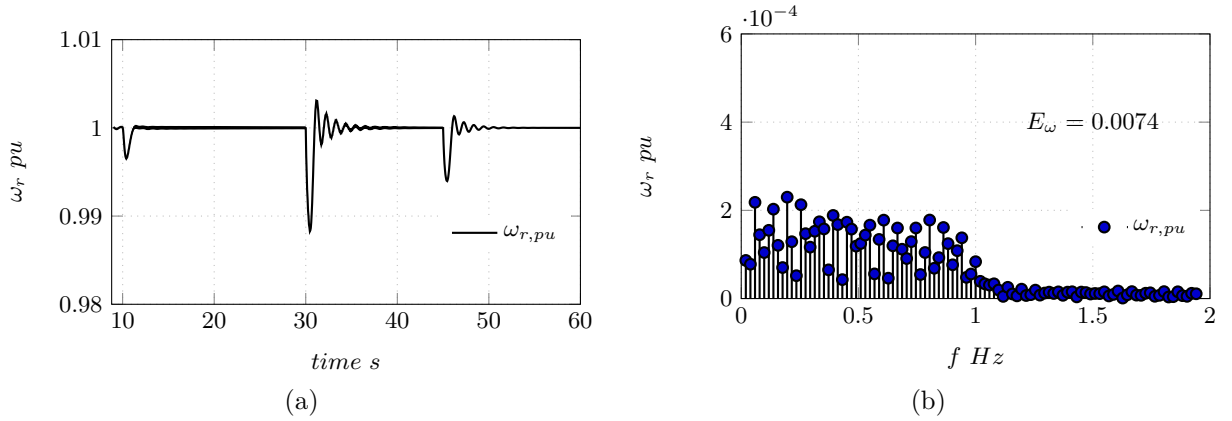

Fig. 10. *Rotor speed of the base case (no WT integrated).*
a Time behaviour.
b Frequency components of the oscillation of ω_r. The energy of the frequency spectrum for the rotor signal is E_ω.

V_{ggt} (Fig. 9(b) at 30 and 45 s).

The rotor angular speed of the GT generator is presented in Fig. 10(a). It can be seen that during the transients it drops up to less than 0.99 pu and shows an oscillatory recovery lasting 5-6 seconds. The frequency spectrum of the rotor speed is also presented where the main component of ω_r is $\omega_{f=0}$ (i.e. the nominal rotor angular speed value). The remaining part of the spectrum is presented in Fig. 10(b), The energy of this spectrum is presented as E_ω[1] and its meaning will be addressed in section 5.3 [36].

5.2. Case II: constant FLEX and WT

An overview of the system waveforms under continuous operation of the WIS at maximum power (fixed S_{FLEX}) is provided in Fig. 11, where the WT power is divided by the system base apparent power ($Sbase$: GT-SG generator rated power) and it is represented in pu. The power quantities

[1]Here, the term energy is used in the sense of signal processing.

for GT and WT are represented by P_{wt}, P_{egt}, Q_{egt} and P_{mgt}, respectively. Additionally, the DC voltage of the grid connected converter of the WT is V_{dcwt}. The GT balances both the fixed load and wind variations, and it is the main responsible for the system stability. After 10 s, the WT and the FLEX load are activated. The gas turbine reduces the generation when the WT produces nominal power at 20 s. The GT compensates the power variations at 30 s (i.e. activation of $S_{FL,2}$), once the WT reduces its injected power. Figure 12 shows the generators rotor angular speed behaviour in the time domain (Fig. 12(a)) and the respective Fourier spectrum of the rotor speed (Fig. 12(b)). Moreover, the energy of the spectrum is also presented. Comparing Fig. 12 and Fig. 10 it can be seen that the intermittent power injected from the WT significantly contributes to increase the low frequency oscillations in the generator rotor speed (as it is confirmed by comparing the corresponding spectral energies) and makes it more irregular. It can also be mentioned that the synchronous GT feeds the reactive load needs as in the first case, since no contribution is taken from the WT. Even though GTs are flexible units, constant load variations might affect their performance, efficiency and increase maintenance requirements.

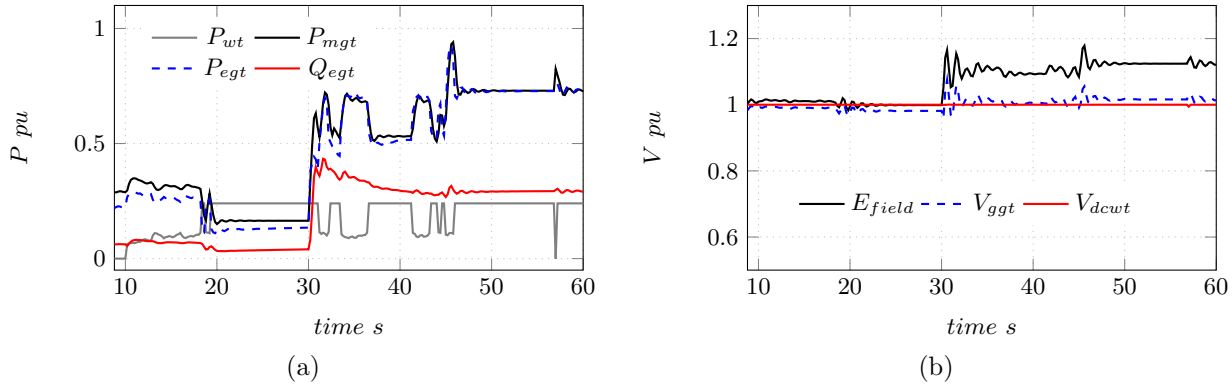

Fig. 11. *System behaviour for Case II (WT integrated, constant FLEX).*
a Mechanical power, active and reactive power of the GT and WT. The apparent power base is $S_{base} = 25$ MVA.
b Field voltage and grid voltage of the GT.

5.3. Case III: FLEX following wind

A new approach is studied in this case: the load is still divided between fixed component FL (which is activated in steps as in the cases above) and flexible component FLEX (the FLEX load now changes following the WT power profile). The inductive share of the load is kept constant for each FL. The flexible load represents an idealization of a water injection pump with smart load management following the renewable generation. Since the wind profile and the turbine characteristics are the same as in the base case, the wind turbine dynamics are not explained in this section. The emphasis is given to the gas turbine response under the new condition. One of the main characteristics is that the starting of the WT and the FLEX smooths the transient at 10 s (shown in Fig. 13(a)). Furthermore, the smart management of the FLEX load mitigates the effect of the load operating transients, reducing the low frequency rotor oscillations. This is confirmed by the corresponding significant reduction in the energy of the spectrum with $E_\omega = 0.0098$ versus $E_\omega = 0.0152$ with constant FLEX (see Fig. 14).

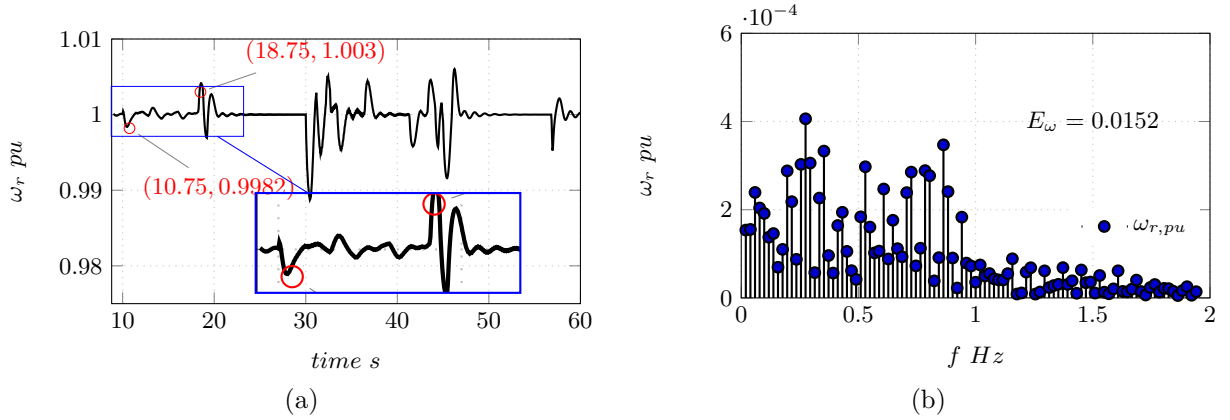

Fig. 12. *Rotor speed behaviour for case II (WT integrated, constant FLEX).*
a Time behaviour.
b Frequency components of the oscillation of ω_r.

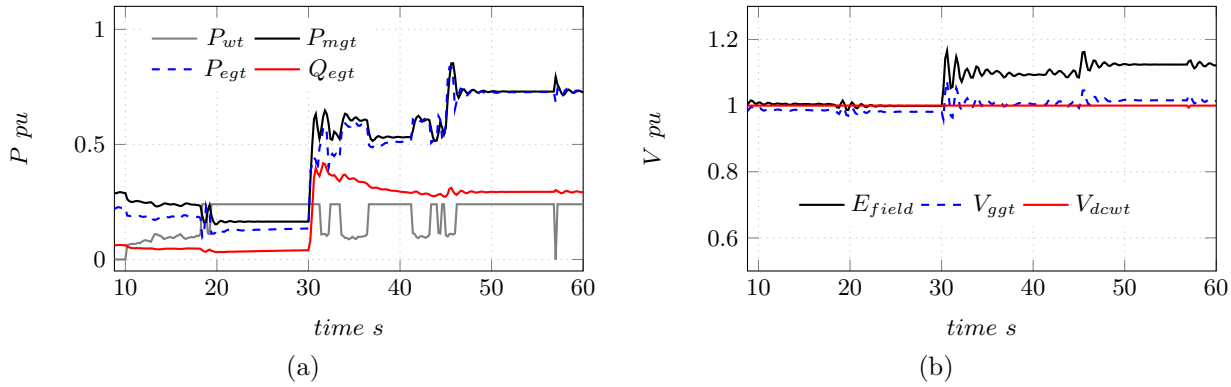

Fig. 13. *System behaviour for Case III (WT and FLEX with same profile).*
a Mechanical power, electrical power and reactive power of the GT and WT. The apparent power base is $S_{base} = 25$ MVA.
b Field voltage and grid voltage of the GT.

5.3.1. FLEX following wind profile: effect of communication delays: A drastic delay (1 s) in the communication and actuation system, resulting in a phase shift between the WT extracted power and the FLEX load profile, is simulated Fig. 15 and Fig. 16. Industrial communication protocols and networks are used to control electrical drives which could be affected in this type of hazardous environments. Additionally, the time response of the actuators or the controllers can be added to this delay. Hence, the goal of this test is to see any problem in the tracking of the reference power of the FLEX and its effects in the system. Again the active power sharing is affected by this disturbance and the rotor experiences variations around the operation point (Fig. 15). Figure 16 shows that the delay produces more oscillations and higher magnitude of the oscillations in the rotor and directly involving the electrical frequency, showing the criticality of poor WT power tracking in the following application.

5.4. Angular speed analysis

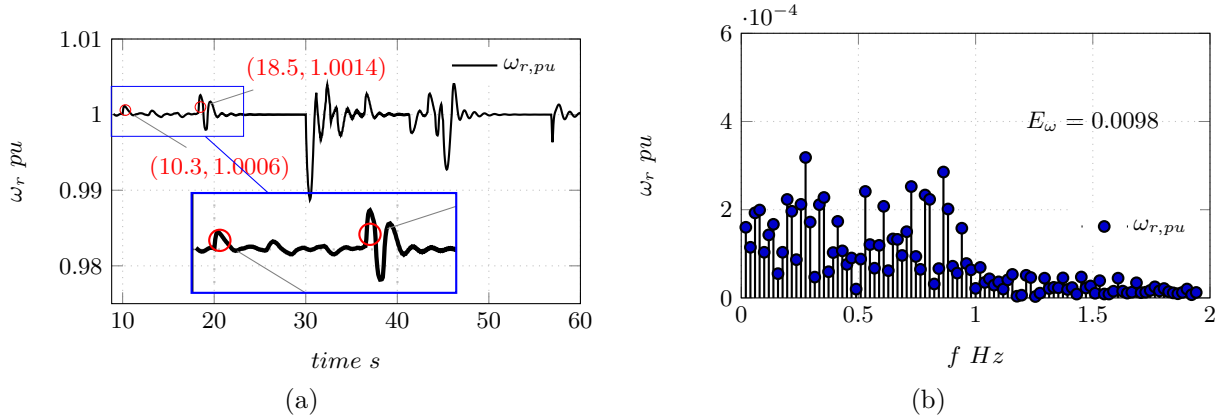

Fig. 14. *Rotor speed behaviour for Case III (WT and FLEX with same profile).*
a Time behaviour.
b Frequency components of the oscillation of f_e.

Table 2 Energy of the spectrum of the angular speed for all the test cases.

Case	Energy ω_r
I	0.0074
II	0.0152
III	0.0098
IV	0.0172

The energy of a signal in a finite band is applied on the rotor angular speed frequency spectrum. This test is carried-out to quantify the degree of influence of the disturbed system: a rotor angular speed signal with lower energy value shows that the rotor speed is less perturbed (i.e. close to the nominal value 1 pu). Table 2 shows the energy values for the four cases described above. Case I represents the simplest behaviour with the lowest energy value. However, the system does not have the WT integrated. The connection of the WT (Case II) introduces severe rotor speed oscillations due to intrinsic wind intermittency. It is possible to conclude that by the application of smart load management the generator rotor angular speed will be less disturbed (e.g. energy value for the case III is less than the energy for case II). Additionally, a possible problem in the communication exemplified by a 1 s delay (case IV) presents the larger energy of the signal value.

6. System damping concept

In order to give an index of the criticality of the penetration of the intermittent WT generation and load dynamics into the O&G isolated electric system, the concept of damping ratio of dynamic systems is used [35]. It is useful to analyse the response on the power sharing of the system. The damping estimation quantifies the changes of the damping coefficient in time domain. The information conveyed by the damping coefficient can be used to set alarms in critical power systems such as O&G isolated grid systems. In this case it is studied on the rotor angular speed of the GT-SG system. The method uses the second order system (3), with $y(t)$ the signal under test (in

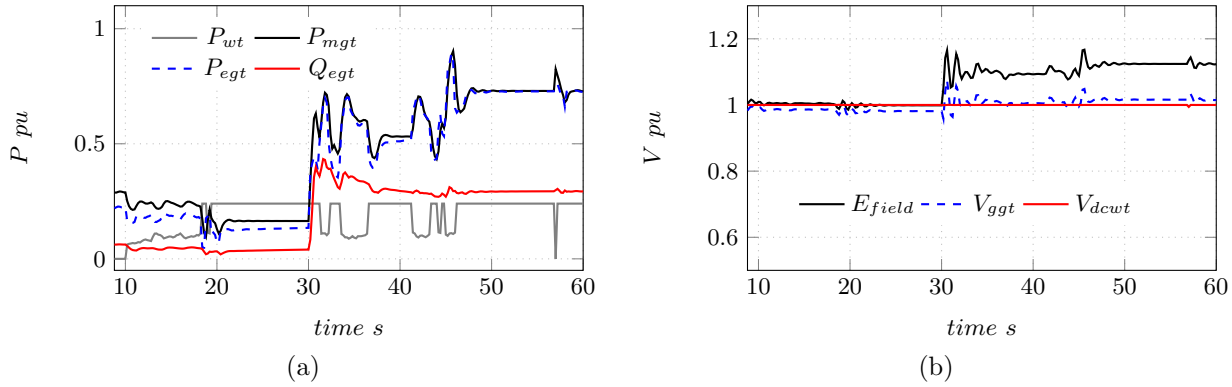

Fig. 15. *System behaviour for Case IV (WT and FLEX with same profile additionally 1 s delay on the FLEX reference).*
a Mechanical power, active and reactive power of the GT and WT. The apparent power base is $S_{base} = 25$ MVA.
b Field voltage and grid voltage of the GT.

this case the rotor speed of the generator), $u(t)$ can be a load demand that excites the system.

$$\frac{d^2y(t)}{dt^2} + 2\rho\omega_n\frac{dy(t)}{dt} + \omega_n^2 y(t) = u(t). \tag{3}$$

In (3) the damping ratio is ρ, the natural frequency of the system is ω_n. Under-damped systems present a $\rho < 1$ and they are the characteristic behaviours studied here.

It is well known from dynamic systems theory that the roots of the characteristic equation (3) are the eigenvalues of the system and they can be obtained as:

$$\begin{aligned} \lambda_{1,2} &= -\rho\omega_n \pm j\omega_n\sqrt{1-\rho^2}, \\ \lambda_{1,2} &= -\alpha \pm j\omega_t, \end{aligned} \tag{4}$$

where ω_t is the oscillation frequency and is different ω_n, $\omega_t = \omega_n\sqrt{1-\rho^2}$. The real part of λ is the attenuation, and the damping ratio can be obtained as $\rho = -\alpha/\sqrt{\alpha^2+\omega_t^2}$.

6.1. Damping estimation method

A simple estimation method has been employed in this work based on the fact that just one synchronous generator is considered and the rotor speed of this SG is the variable under test. First a transient event detector algorithm based on the first derivative has been applied [37]. The step changes in the system are tracked by the first derivative $Y_1(n)$ in (5). $Y(n)$ represents the the rotor speed discrete signal, where n is the discrete sample. Once the absolute value of the derivative crosses a threshold value then the detector gives a true logic signal which helps to start the storage of the signal in a buffer with size τ s.

$$Y_1(n) = Y(n) - Y(n-1) \tag{5}$$

After all the samples in the window of the oscillation have been stored the mean value is evaluated and subtracted from the signal in order to obtain a impulse response signal. The least squares

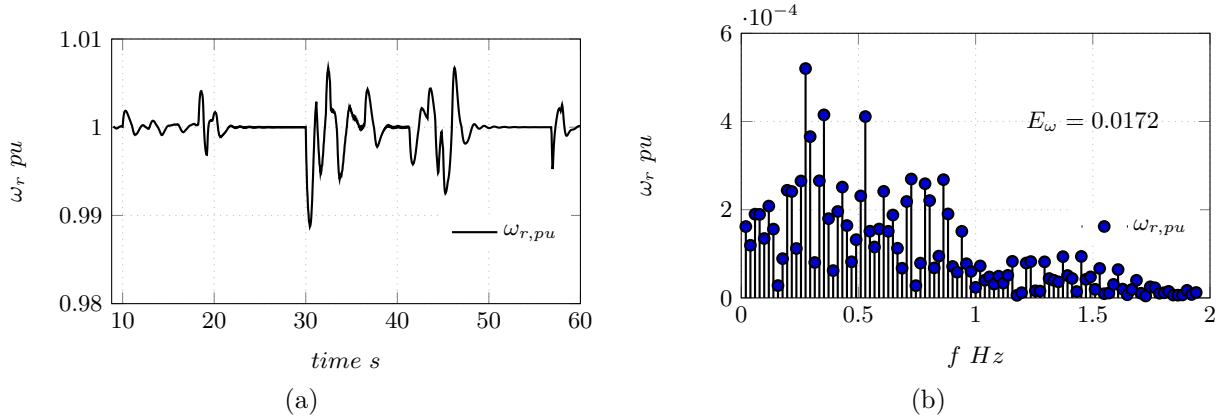

Fig. 16. *Behaviour of the rotor speed for Case IV (WT and FLEX with same profile additionally 1 s delay on the FLEX reference).*
a Time behaviour.
b Frequency components of the oscillation of f_e.

algorithm is applied to the samples in order to obtain ρ and ω_t as done in [38]. In order to obtain the fitting of the curve, first, the discrete model of (3) is obtained in (6). In (6) the input has been set to zero. The parameters of the polynomial have a relation with the continuous parameters of (3). The least square model to estimate the parameters is $y = H\theta$, where θ is a vector with the parameters a_1 and a_2 to be estimated, H is the matrix with the known terms [36]. In (7) $l - 2$ is the length of the sampled data.

$$y_k + a_1 y_{k-1} + a_2 y_{k-2} = 0 \tag{6}$$

$$\begin{bmatrix} y_k \\ y_{k-1} \\ \vdots \\ y_{k-l} \end{bmatrix} = \begin{bmatrix} y_{k-1} & y_{k-2} \\ y_{k-2} & y_{k-3} \\ \vdots & \vdots \\ y_{k-(l+1)} & y_{k-(l+2)} \end{bmatrix} \begin{bmatrix} a_1 \\ a_2 \end{bmatrix} \tag{7}$$

The damping and oscillation frequency are obtained as the roots of the polynomial formed with the parameters in (6) and converted to the continuous domain by the use of the Tustin's approximation [34]. With the poles in Laplace domain $(s + \lambda_1)(s + \lambda_2) = 0$ the natural frequency and damping coefficient are calculated based on the definition used in (4).

6.2. Damping estimation for the WIS and WT penetration

The effect of WT and FLEX dynamics is evaluated with the damping ratio estimated from the GT-SG rotor speed signal. Fig. 17(a) shows the first derivative of the rotor angular speed of the GT-SG and the threshold used to detect the disturbances. In this case a threshold of 11×10^{-4} pu has been used, the window to estimate the damping ratio and the frequency of oscillation is $\tau = 2.5$ s, with a sampling time of 0.1 s as used in [34]. Fig. 17(b) presents the steps of the estimated ρ and Fig. 17(c) the estimation of the oscillation frequency of the rotor signal ($f_{oscillation}$ for case II and case III), the points represent the estimation detection which triggers the storage of the signal to estimate. In case III the FLEX is following the profile of the WT generation and it has ideal

tracking without delays. Around 18 s a 14% damping is obtained for case III and 7% damping for case II. After this last window another disturbance is detected around 30 s which is a result of the S_{FLEX2} activation (see Fig. 13(a) after 30 s) this results in a $\rho_{II} = 1.8\%$ for case II and $\rho_{III} = 5.8\%$ for case III, the next power disturbance is detected before 35 s and both damping values are around 40%. Around 35 s the event is detected and is produced by the maximum power injection by the WT. It is important to note the reduction of ρ_{II} to 17% and ρ_{III} to 22% due to the nominal power injected by the WT. After 40 s a disturbance is detected and is associated to the MPPT operation mode of the WT where ρ_{II} is having two threshold activations ($\rho_{II} = 10$ and 8.2%), while $\rho_{III} = 10\%$ just after 44 s. Last region after 55 s activates the estimation again when two events are encountered, namely S_{FLEX3} activation and WT switches from MPPT to nominal power generation ($\rho_{II} = 36\%$ and $\rho_{III} = 44\%$). It can be concluded that the use of the SLM shows better performance in terms of increased damping than the use of a WIS without wind power profile tracking.

Finally, to compare the behavior under a 1 s communication delay between the FLEX and the WT, the analysis of the corresponding damping coefficients and the oscillations is presented in Fig. 18. It is easy to see the multiple steps on the damping plot Fig. 18(b) which show the work of the detector. Moreover, the derivative of the rotor speed (Fig. 18(a)) shows the increased disturbance in the spikes that represent the transients on the rotor speed. The less affected region is between the 30 s to 50 s, in this part it is shown how ρ is close to 20%. Between 45-55 s there is a large disturbance that produces a very low ρ which results from the MPPT of the WT. The frequency estimated for the oscillations of the power are shown in Fig. 18(c), where low frequency disturbances (in agreement with [34, 35]) have been estimated.
The latter example further proves the criticality of the delay in the WT power following by the FLEX load SLM. This increases the interest in additional research on communication-less methods, which rely only on local measurement at P_{FLEX}, potentially avoiding the problems of the communication delays. The validation of such techniques is, however, outside the scope of the paper and is left open for future work.

7. Conclusion

The use of wind power to supply oil and gas installation has been recently regarded as an option to make the sector less polluting and more sustainable. Previous studies have mostly investigated the amount of CO2 and NOx emissions that can be avoided by wind integration into O&G platforms or the voltage and frequency stability limit. One aspect that has not been covered so far is the possible arise of electro-mechanical oscillations in the O&G power system, due to the inherent wind intermittency and consequent higher power imbalances. This paper shows that under the traditional scenario of inflexible loads, the use of wind power determines a significant increase of low-frequency oscillations in the range 0.1- 2 Hz, which are considered especially critical in power systems from the standpoint of rotor angle stability.

On the other hand, the paper considers that the increasing share of controllable loads, (e.g. water injections systems) usually connected to variable speed drives in O&G installations, make the idea of managing the load attractive, in order to keep the system power balance.
Several cases were discussed to test the impact on the power system when a fixed and a combination of a fixed and flexible load are connected to the platform. The results indicate that controlling

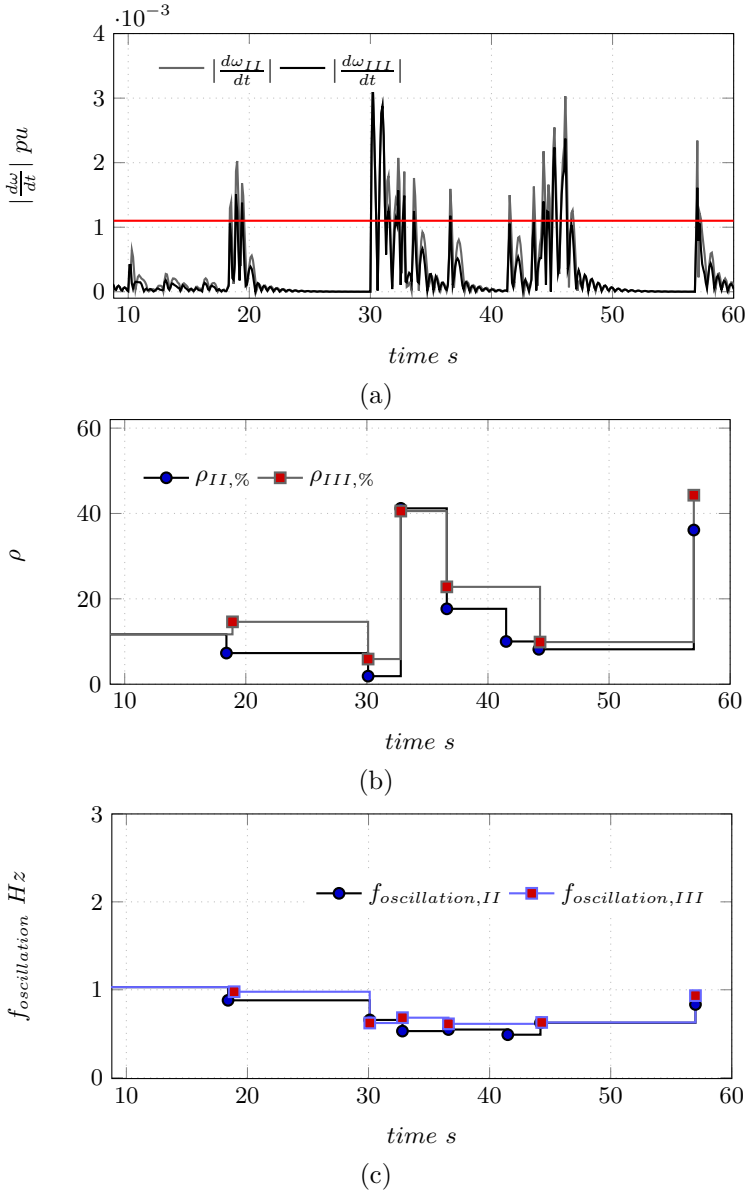

Fig. 17. *Behaviour of the damping estimation for cases II and III (WT with constant FLex and WT with FLEX following same profile).*
a Derivative of the rotor speed.
b Damping coefficient in percentage.
c Frequency oscillation of the rotor speed transients $f_{oscillation}$ in Hz.

the load demand to follow the wind variations, results in an improved response in terms of lower average rotor speed deviations and better power balance between generation and consumption with respect to the case of a constant fixed load (See the zoomed area in Fig. 12 and Fig. 14), possibly allowing a larger share of wind penetration. The presented case, with perfect correspondence between wind generation profile and load control, should be considered as a proof of concept of the proposed idea. A more realistic situation considering a time delay in the load variations with

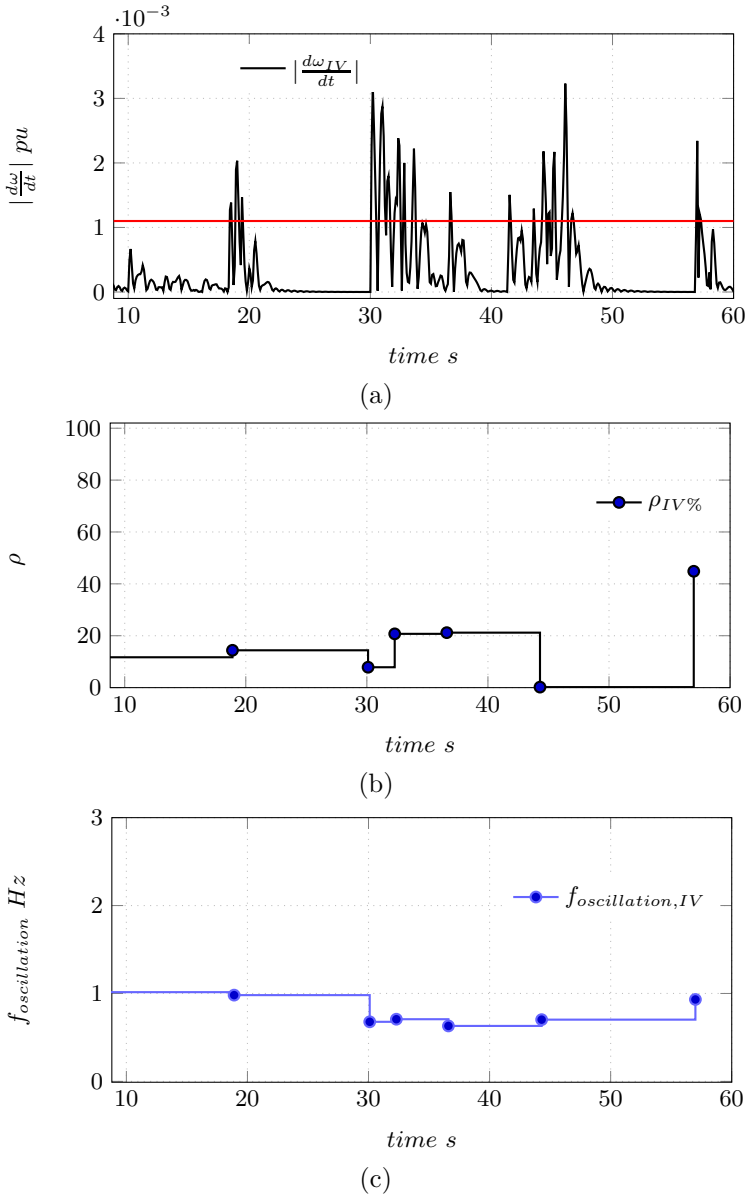

Fig. 18. *Behaviour of the damping estimation forfor delay test (WT and FLEX with same profile additionally 1 s delay on the FLEX reference).*
a Derivative of the rotor speed.
b Damping coefficient in percentage.
c Frequency oscillation of the rotor speed transients $f_{oscillation}$ in Hz.

respect to the wind power profile (because communication, actuators and the controllers have a finite actuation time) has also been presented. The criticality of such delay, which can hinder the advantages of the flexible load management and worsen the system performance in terms of increased rotor angle oscillations, has been highlighted. On this respect, techniques reducing such delay, including communication-less methods, where the load control is based on local frequency measurements rather than on the actual power information received from the WT, can be consid-

ered. In addition, this paper has proposed a method that estimates the system damping and rotor speed oscillations as a consequence of load variations and the effects of the WT power injection. This recursive algorithm, based on the first derivative of the rotor speed, automatically calculates the damping levels after each detected event such as load activations. The algorithm is effective and simpler compared to previous methods using higher order models and it can be used to alert on critically low damping conditions in sensitive systems such as O&G applications.

8. References

[1] M. Jafar, P. Vaessen, A. Yanushekvich, Y. Fu, R. Marchall, T. Bosman, M. Irvine, and Y. Yang, "Hybrid grid, towards a hybrid ac dc transmission grid," *DNV GL strategic research and innovation position paper*, no. 2, 2015.

[2] A. R. Ardal, K. Sharifabadi, O. Bergvoll, and V. Berge, "Challenges with integration and operation of offshore oil amp; gas platforms connected to an offshore wind power plant," in *2014 Petroleum and Chemical Industry Conference Europe*, June 2014, pp. 1–9.

[3] K. M. Lorentzen, A. Atle Rygg, S. Kamran, and T. Marvin, "Integrating offshore wind power and multiple oil and gas platforms to the onshore power grid using vsc-hvdc technology." in *Marine Technology Society Journal*, vol. 48, 2014, pp. 31–44.

[4] M. L. Kolstad, K. Sharifabadi, A. Rygg Ardal, and T. Undeland, "Grid integration of offshore wind power and multiple oil and gas platforms." in *OCEANS-Bergen IEEE*, 2013.

[5] M. J. I., E. V. Oyslebo, and M. Korpas., "Electrification of offshore petroleum installations with offshore wind integration." in *Renewable energy 50*, 2013, pp. 558–564.

[6] A. A. Rygg, T. Undeland, and K. Sharifabadi, "Voltage and frequency control in offshore wind turbines connected to isolated oil platform power systems." in *Energy Procedia*, vol. 24, no. 24, 2012, pp. 229–236.

[7] H. G. Svendsen, M. Hadiya, E. Oyslebo, and K. Uhlen, "Integration of offshore wind farm with multiple oil and gas platforms." in *IEEE PowerTech*, 2011, pp. 1–3.

[8] W. He, K. Uhlen, M. Hadiya, Z. Chen, G. Shi, and E. del Rio, "Case study of integrating an offshore wind farm with offshore oil and gas platforms and with an onshore electrical grid," *Journal of Renewable Energy*, vol. 2013, pp. 1–10, 2013.

[9] W. He, J. Gunnar, A. Tiit, O. Freydar, H. Tor D, M. Korpas, T. Trond, E. Jale, k. Uhlen, and J. Emil, "The potential of integrating wind power with offshore oil and gas platforms." in *Wind Engineering 34*, 2010, pp. 125–137.

[10] M. Korpas, L. Warland, W. He, and J. O. Tande, "A case-study on offshore wind power supply to oil and gas rigs." *Energy Procedia*, no. 24, pp. 18–26, 2012.

[11] K. Prasertwong, N. Mithulananthan, , and D. Thakur, "Understanding low-frequency oscillation in power systems," *International Journal of Electrical Engineering Education*, vol. 3, no. 47, pp. 248–262, 2010.

[12] J. V. Milanovic, ""damping of the low-frequency oscillations of the generator: dynamic interactions and the effectiveness of the controllers."," in *IEE Proceedings-Generation, Transmission and Distribution*, 2002, pp. 753–760.

[13] I. R. Smith, V. V. Vadher, and J. G. Kettleborough, "Small oscillator stability of a synchronous machine." in *Advances in Power System Control, Operation and Management, APSCOM-91, International Conference on. IET*, 1991.

[14] Y. Yu, Y. Shen, X. Zhang, J. Zhu, and J. Du, ""the load oscillation energy and its effect on low-frequency oscillation in power system."," in *Electric Utility Deregulation and Restructuring and Power Technologies (DRPT), 2015 5th International Conference on. IEEE*, 2015.

[15] J. Qazem, Q. Naman, and M. Shamaseen, "Effects of low frequencies on three phase induction motor performance operating in close proximity to rated speed," *Am. J. Applied Sci*, vol. 4, pp. 284–293, 2007.

[16] M. Lasantha and D. Flynn, "Frequency dynamics during high ccgt and wind penetrations," in *Power Engineering Conference (AUPEC), 2011 21st Australasian Universities. IEEE*, 2011.

[17] J. G. Slootweg and W. L. Kling, "The impact of large scale wind power generation on power system oscillations," *Electric Power Systems Research*, pp. 9–20, 2003.

[18] Offshore-Magazine, "2015 worldwide survey of subsea processing: separation, compression and pumping systems." in *INTECSEA WorleyParsons Group*, 2015.

[19] J. Silva, M. Jafar, A. Marichalar, and E. Tedeschi, "Integration of wind power to supply water injection systems as controllable loads in offshore oil and gas facilities," in *Offshore Energy & Storage Symposium (OSES 2016)*, July 2016, pp. 1–9.

[20] S. Norway, "Norway emissions," http://ssb.no/en/natur-ogmiljo/statistikker/klimagassn/aar-forelopige/2016-05-20, 2015, [Online; accessed 22-Jun-2016].

[21] N. Anderson, *Power system stability*. New York: John Wiley & Sons, Inc., 2001.

[22] W. Leonhard, *Control of Electrical Drives*, 3rd ed. United States of America: Springer, 2001.

[23] J. Machowski, J. W. Bialek, and J. R. Bumby, *Power system dynamics, stability and control*, 2nd ed. New Delhi: Wiley, 2008.

[24] P. Kundur, *power System Stability and Control*. United States of America: McGraw-Hill, 1993.

[25] K. Bonfert, *Betriebsverhalten der Synchronmaschine*. Berlin: Springer-Verlag, 1967.

[26] K.-J. Astrom, *PID Controllers: Theory, Design, and Tuning*, 1995.

[27] Petrowiki, "Gas lift," http://petrowiki.org/Gas_lift., 2016, [Online; accessed 18-Nov-2016].

[28] Rigzone., "How does water injection work?" http://www.rigzone.com/training/insight.asp?insight_id=341&c_id=4, 2015, [Online; accessed 18-Nov-2016].

[29] T. Van-Cutsem and C. Vournas, *Voltage stability of electric power systems*. Boston: Kluwer academic publishers, 2001.

[30] Statoil, "Statoil to build the wold's first floating wind farm: Hywind scotland," https://https://www.statoil.com/en/news/hywindscotland.html, 2017, [Online; accessed 1-Jun-2017].

[31] J. A. Baroudi, V. Dinavahi, and A. M. Knight, "A review of power converter topologies for wind generators," *Renewable Energy*, vol. 32, no. 14, pp. 2369 – 2385, 2007.

[32] R. Melicio, V. Mendes, and J. Catalao, "Power converter topologies for wind energy conversion systems: Integrated modeling, control strategy and performance simulation," *Renewable Energy*, vol. 35, no. 10, pp. 2165 – 2174, 2010. [Online]. Available: http://www.sciencedirect.com/science/article/pii/S0960148110001114

[33] L. Harnefors, M. Bongiorno, and S. Lundberg, "Input-admittance calculation and shaping for controlled voltage-source converters," *Industrial Electronics, IEEE Transactions on*, vol. 54, no. 6, pp. 3323 –3334, dec. 2007.

[34] P. Korba, "Real-time monitoring of electromechanical oscillations in power systems: first findings," *IET Generation, Transmission Distribution*, vol. 1, no. 1, pp. 80–88, January 2007.

[35] J. Turunen, J. Thambirajah, M. Larsson, B. C. Pal, N. F. Thornhill, L. C. Haarla, W. W. Hung, A. M. Carter, and T. Rauhala, "Comparison of three electromechanical oscillation damping estimation methods," *IEEE Transactions on Power Systems*, vol. 26, no. 4, pp. 2398–2407, Nov 2011.

[36] R. F. Stengel, *Optimal control and estimation*. New York: Dover, 1994.

[37] N. M. Arzeno, Z. D. Deng, and C. S. Poon, "Analysis of first-derivative based qrs detection algorithms," *IEEE Transactions on Biomedical Engineering*, vol. 55, no. 2, pp. 478–484, Feb 2008.

[38] J. Thambirajah, N. F. Thornhill, and B. C. Pal, "A multivariate approach towards interarea oscillation damping estimation under ambient conditions via independent component analysis and random decrement," *IEEE Transactions on Power Systems*, vol. 26, no. 1, pp. 315–322, Feb 2011.

9. Appendices

9.1. Parameters of the WT system

The converter of the wind turbine has power rate of 6 MVA, a rated voltage 3.3 kV a designed inductor $L_{wt} = 0.1309$ pu, with a resistor $R_{wt} = 0.004\ pu$ for a switching frequency of $f_{sw,wt} = 4$ kHz. The DC link capacitor is $C_{dc,wt} = 43.38\ \mu$F. The internal PI controller per unit gains are the proportional gain $k_{pi} = 0.556$ pu and the integrator gain $k_{ii} = 5.333$ pu. The DC link controller has a PI structure with per unit proportional gain $k_{p,dc} = 1.9052$ pu and the integral gain $k_{i,dc} = 423.36$ pu.

9.2. Parameters of the FLEX

The converter of the FLEX has power rated of 3 MVA a rated voltage of 13.472 kV, a designed inductor $L_{flex} = 0.13$ pu, with a resistor $R_{flex} = 0.004$ pu for a switching frequency of $f_{sw,wt} = 4$ kHz. The DC link capacitor is $C_{dc,flex} = 0.2636$ pu. The internal PI controller per unit gains are the same as the designed for the WT.

9.3. Parameters of the GT and SG

The GT has a first order model with time constant $T_{gt} = 0.25$ s, the controller is a PI with just a proportional gain in pu $k_{p,gt} = 14.8$ pu. The inertia used in the SG is $H = 3.7$ s, the per unit values of the SG are the resistor $R_{sg} = 0.002$ pu, the inductive transient reactance$X_{L,sg} = 0.3$ pu, the damping gain is $k_{damp} = 7.0422$, pair of poles = 20, electrical frequency $f_e = 50$ Hz, the power rate is 25 MVA, the line to line base voltage $V_{base,L-L} = 13.472$ kV. The excitation system and parameters are taken from [23].

9.4. Parameters cable and transformers

The cable resistance is $R_c = 0.01273\ \Omega/km$, the reactance is $X_c = 0.0734\ \Omega/km$.
The transformer T_1 uses the following rates: $V_1/V_2 = (3.3\ kV)/(33\ kV)$, apparent power rate 6 MVA, series resistor $R = 0.0031$ pu, series reactor $X_L = 0.1100$ pu. The transformer T_2 uses the following rates: $V_1/V_2 = (33\ kV)/(11\ kV)$, apparent power rate 6 MVA, and uses the same impedance in per unit as T_1.